Development of a Novel Direct-Drive Tubular Linear Brushless Permanent-Magnet Motor

Won-jong Kim and Bryan C. Murphy

Abstract: This paper presents a novel design for a tubular linear brushless permanent-magnet motor. In this design, the magnets in the moving part are oriented in an NS-NS—SN-SN fashion which leads to higher magnetic force near the like-pole region. An analytical methodology to calculate the motor force and to size the actuator was developed. The linear motor is operated in conjunction with a position sensor, three power amplifiers, and a controller to form a complete solution for controlled precision actuation. Real-time digital controllers enhanced the dynamic performance of the motor, and gain scheduling reduced the effects of a nonlinear dead band. In its current state, the motor has a rise time of 30 ms, a settling time of 60 ms, and 25% overshoot to a 5-mm step command. The motor has a maximum speed of 1.5 m/s and acceleration up to 10 *g*. It has a 10-cm travel range and 26-N maximum pull-out force. The compact size of the motor suggests it could be used in robotic applications requiring moderate force and precision, such as robotic-gripper positioning or actuation. The moving part of the motor can extend significantly beyond its fixed support base. This reaching ability makes it useful in applications requiring a small, direct-drive actuator, which is required to extend into a spatially constrained environment.

Keywords: Direct-drive DC motor, linear actuator, permanent-magnet motor, real-time digital control, tubular motor.

1. INTRODUCTON

The objective of the work described in this paper is to develop a novel linear actuator capable of fast, smooth, precise positioning with a 10-cm actuation range. The direct-drive tubular linear brushless permanent-magnet motor (LBPMM) shown in Fig. 1 has a slotless stator to provide smooth translation without cogging. This design choice sacrifices the higher force capabilities that would be possible with iron slots in the stator in favor of smooth actuation. Applications for this type of actuator include precision positioning and robotic actuation needs. Linear actuators are used in robot end-effectors such as dexterous hands [1] and as the final link in multi-link robotic arms. Budig discusses many types of applications for which linear motors are appropriate [2].

Some linear actuators are comprised of hydraulic or pneumatic rams, which are good for non-precision applications requiring high force. Others use an electric rotary motor with a lead screw or other linkage to convert rotary motion to linear translation, which has serious complications including backlash and increased mass of the moving part due to connecting linkages or gears. Hence, the LBPMM, which is comprised of permanent magnets and current-carrying coils, is especially suited for precision positioning applications.

There have been many contributions in the field of LBPMM's and other direct-drive systems, in which the load is propelled directly by the motor. LBPMM's

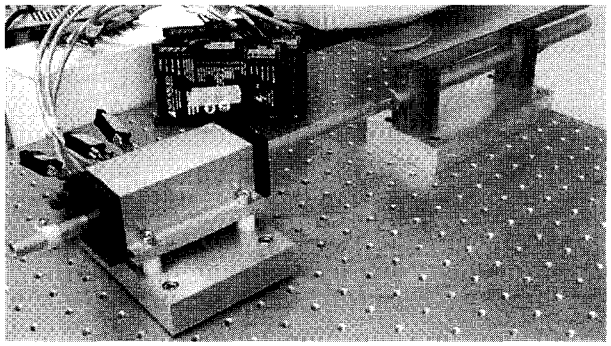

Fig. 1. Assembled tubular linear motor mounted on a precision optical table shown with brass tube connected to the LVDT at right. The permanent magnets are within the brass tube. The amplifiers can be seen in the back.

Manuscript received April 1, 2004; accepted June 9, 2004. Recommended by Editor Keum-Shik Hong.

Won-jong Kim is with the Department of Mechanical Engineering, Texas A&M University, 3123 TAMU, College Station, Texas 77843-3123 USA (e-mail: wjkim@mengr.tamu.edu).

Bryan Murphy is with The Boeing Company, International Space Station, Loads, Dynamics, and Mechanisms division, 13100 Space Center Blvd, Houston, TX 77059 USA (e-mail: Bryan.C.Murphy@boeing.com)

are commonly used in single- and multi-degree-of-freedom precision positioning applications. Lequesne investigated a number of performance criteria for permanent-magnet linear motor designs with translation range from 5 to 20 mm [3]. Kim and Trumper, et. al demonstrated that a six-degree-of-freedom planar LBPMM could be used for precision nanopositioning [4,5]. This setup consists of current-carrying coils contained within a stationary base beneath a platen comprised of matrices of permanent magnets. When energized, the coils levitate the platen and allow significant translation and rotation in the plane of the base plate.

Berhan, et al. discussed the use of a Halbach magnet array [6] in a novel ironless tubular LBPMM [7,8]. The Halbach array is implemented in the form of axisymmetric octagonally-oriented rectangular permanent magnets, which approximate a cylindrical Halbach array. The primary differences between the cited motor and the proposed design is that the proposed motor has a simpler mover made up of cylindrical permanent magnets, is more compact in size, and is much easier in construction.

Ishiyama, et al. designed a tubular LBPMM that can be used to drive a carriage in an image reading device and other applications [9]. This design entails an array of hollow radially-magnetized permanent magnets, with the poles of each magnet aligned with the attractive poles of the adjacent magnets. This configuration is repeated to produce a relatively long tubular array of magnets, which constitutes the fixed part of the motor. The primary differences between this design and the design proposed herein are the magnetization direction of the magnets and the configuration of the motor. The cited design also embodies a fixed array of magnets, with the outer coils as the moving part. This is substantially different from the motor discussed in this paper, as in the latter the tube, which encompasses the permanent magnets, is free to extend out well beyond the support of the base.

Zhu, et al. constructed a tubular LBPMM and discussed cogging minimization [10]. In this design multiple motor topologies are discussed. Radially-magnetized magnets similar to those in [9] and axially-magnetized magnets as in the authors' design were both proposed as options for the embodiment. This design uses an iron core in the stator, which instigates cogging forces into the system. The primary performance goal discussed in [10] is to maximize the force-per-current and force-per-volume ratios. In the proposed design herein, while output force is of appreciable concern, the primary desire is for precise positioning.

Liaw, et al. developed an LBPMM with robust position control [11]. Shieh and Tung designed a controller for an LBPMM used in a manufacturing system [12]. Brückl discussed the use of a linear motor for ultra-precision machine tools [13], which is also a possible application for our design. Basak and Shirkoohi used a software package to compute the magnetic field in DC brushless linear motors with NdFeB magnets [14]. Lee demonstrated a cylindrical linear motor design using toothed sections which makes assembly easier and prevents overheating [15]. Trumper, et al. discussed electromagnetic arrays capable of generating field patterns in two and three dimensions by varying current density in the winding [16]. Ishiyama presented a stator design for a cylindrical linear motor in which opposing faces of ring shaped permanent magnets are adjacent and positioned close to each other using a tightening mechanism [17]. Akmese, et al. described computer-aided analysis of machine parameters and the magnetic cogging force using finite element techniques [18]. Eastham, et al. discussed the optimum design of brushless tubular linear machines [19].

The concepts given in the aforementioned papers, particularly those discussed in [7-10], incorporate qualities similar to the design proposed here, but with significant differences. The proposed design allows for compact actuation of a slender cylindrical tube, which is free to extend beyond the support base. As the design is ironless and slotless, there is no cogging, which allows smooth translation. The downside of this ironless design is that there is no iron yoke to concentrate the magnetic field, so the efficiency suffers. The compact design of the motor makes it applicable to space-constrained robotics applications. The potential resolution of the system lends itself to applications in precision positioning.

In the following sections, a presentation of the electromechanical design is given with the governing equations and motor sizing discussed. Next, the design of controllers for particular motion requirements is presented, as well as the steps taken to optimize the controllers for two specific robotic-actuation needs. Several experimental results are given illustrating the system response to various inputs, some including externally applied loads. The maximum force for which the motor is capable is also determined. This work is also discussed in detail in [20].

2. ELECTRO-MECHANICAL DESIGN

2.1. Design concept

Fig. 2 represents the conceptual configuration without particular dimensions assigned to the magnets and coils. Cylindrical permanent magnets are placed in an NS-NS—SN-SN fashion with spacers between pairs. The magnet pitch is required to match the coil pitch, and arranging magnets (which were conveniently available) together in pairs allowed the magnet

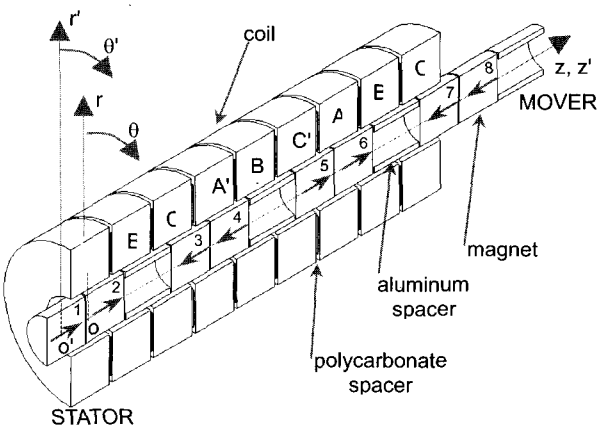

Fig. 2. Section view of coils and magnets with brass tube hidden. Coordinates are given for the mover frame (primed frame) as well as the stator frame (unprimed frame) that is stationary in space.

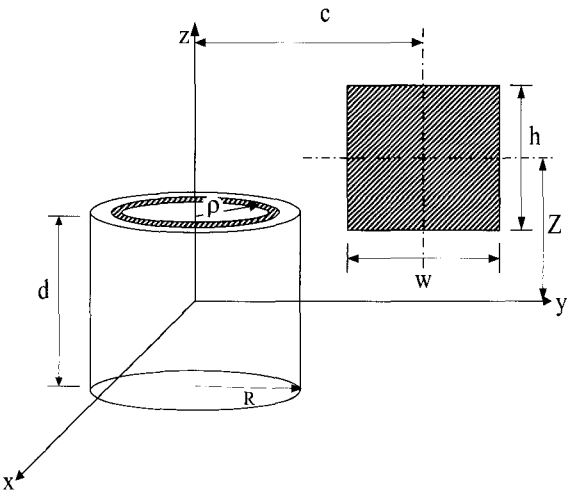

Fig. 3. Parameters between permanent magnet (left) and current-carrying coil (upper right). The coil is represented with a rectangular cross-section.

pitch to match the coil pitch. The magnets are fixed within a freely sliding brass tube which constitutes the mover. Electromagnetic coils are configured in three phases labeled A, B, and C. Each coil has one lead from the outermost turn and one from the innermost turn. The coils are arranged in sequence such that every third coil is in the same phase. The coils constitute the stator, and the mover is placed within the stator. As the coils are powered, they exert a force upon the permanent magnets according to the Lorentz force equation, which causes translation of the mover.

The length (along the z-axis) of the magnets is set to be equal to that of the coils. Therefore the required design parameters are the length of the magnets/coils, the outer radius of the magnet and the inner radius of the coil (this pair determines the air gap between them), and the outer radius of the coil. The magnet array is fixed within a brass tube, space for which must be accommodated in the air gap between the magnet and coil arrays.

2.2. Motor force calculation and sizing

To determine the particular values for the design parameters, some quantified desired performance criteria must be established. In this case, the conceptual design guarantees the smooth translation requirement, as there are no iron slots, which would introduce cogging. The remaining performance parameter of interest is the maximum output force. The Lorentz force equation, $\boldsymbol{f} = \int (\boldsymbol{J} \times \boldsymbol{B})\, dV$ governs the interaction of the coil current and permanent magnet. The output force is the volumetric integral of the cross product of the current density in the coil with the magnetic flux density generated by the permanent magnet over the whole coil volume.

The force of primary interest is the interaction of a single magnet with a single coil current. Upon further expansion and simplifications due to symmetry, the Lorentz force equation becomes (1). Some geometric parameters are given in Fig. 3. A thorough derivation is given in [20], in which material from [21,22] was quite helpful.

The coil inductance and resistance are 0.500 mH and 0.552 Ω, respectively, per coil. A maximum current of 3 A flow through each coil. The magnets chosen for evaluation were cylindrical neodymium iron boron (NdFeB) magnets. Their maximum energy product (BH_{max}) is 0.4 MJ/m^3 (50 MGOe). The magnets chosen are 10.0-mm (0.395") in diameter,

$$f_z = \left(\frac{J(\mu_0 M)}{4\pi}\right) \int_{c-\frac{w}{2}}^{c+\frac{w}{2}} \int_{Z-\frac{h}{2}}^{Z+\frac{h}{2}} \int_0^{2\pi} \frac{d}{dr} \left[\int_0^R \int_0^{2\pi} \frac{\rho}{\sqrt{(z-d/2)^2 + r^2 + \rho^2 - 2\, r\, \rho \cos(\theta - \phi)}} d\theta\, d\rho \right. \tag{1}$$

$$\left. \ldots - \int_0^R \int_0^{2\pi} \frac{\rho}{\sqrt{(z+d/2)^2 + r^2 + \rho^2 - 2\, r\, \rho \cos(\theta - \phi)}} d\theta\, d\rho \right] r\, d\phi\, dz\, dr$$

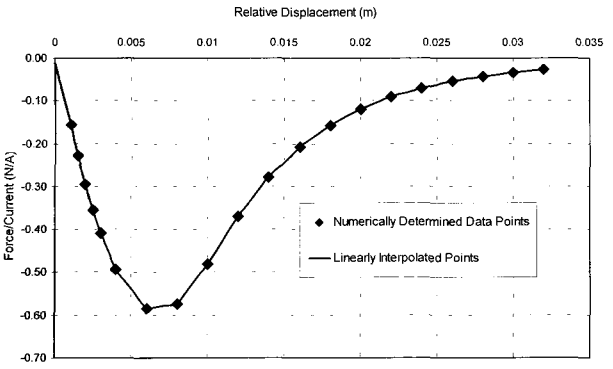

Fig. 4. Theoretical force per current as a function of relative displacement for one magnet with one coil.

9.53-mm (0.375") long, and have a minimum remanence of 1.20 T. To allow adequate space for the 11.1-mm (7/16") O.D. (outer diameter) brass tube to house the magnets and slide freely without contact within the coils, the I.D. (inner diameter) of the coils was chosen to be 12.2 mm, with an O.D. of 33.2 mm. The length (in the z-direction) was selected to be 9.53 mm to match that of the magnets. Using AWG #21 wire, 179 turns of wire fit within the design envelope.

Based on these dimensions, the force per current between a single magnet and single coil as a function of relative displacement (Z) can be determined using (1). MathCAD was used to solve for this force per current for numerous values of Z. These results are illustrated in Fig. 4. The points given in the figure are from iterations solved in MathCAD. The lines connecting the points into a continuous line are from linear interpolation between these points.

2.3. Mechanical design

The stator consists of nine coils (three per each phase), corresponding to 1½ pitches. To provide the desired travel range of 10-cm, several pitches of magnets are included, so that there are always magnets within appreciable force range on both sides (axially) of each coil. Aluminum spacers were used between pairs of magnets so that the magnets could be glued together. The magnets and spacers were glued in place by coating PC-7 epoxy on the outer surfaces. The magnet pitch consisting of four magnets with two spacers is 63.3 mm. A brass tube was chosen to house the magnets and spacers. The tube has an 11.1-mm (7/16") O.D., wall thickness of 0.356 mm (0.014") and is 305 mm (12.0") in length. The magnets and spacers are positioned in the brass tube in an NS-NS—SN-SN orientation. The magnets within the brass tube will translate through the nine-coil assembly, as shown in Fig. 2. Nylon bearings which support the brass tube are held in Delrin housings fixed to both ends of the stator.

When gluing the coils together face-to-face, 0.787-mm-thick multi-layer polycarbonate spacers were used to leave a gap between coils for the lead wire from the innermost coil winding to run along the face of the coil to the outside of the coils. A notch was cut from the inner diameter to the outer diameter of each of the spacers to leave room for the lead wire. The spacers were trimmed so that the inner diameter of the spacers was larger than that of the coils and so that the outer diameter of the spacers was smaller than that of the coils. This allowed the brass tube to slide freely through the coils, and also left room for the wire leads on the outside of the coils to be wrapped around to the appropriate location. The effective thickness of the added polycarbonate spacer (including the glue line on both faces) was 1.03 mm. Thus, the stator pitch consisting of six coils with six spacers is 63.3 mm, the same as the magnet pitch.

2.4. Commutation

In order to provide balanced three-phase current to the motor, a commutation equation relating force and current based on position was required. For convenience, the coordinate convention designated in Fig. 2 was chosen to correlate with that defined in [8] so that the commutation equation would be applicable without significant modification. The commutation equation from said paper is given in (2), where C replaces a quotient of geometric parameters.

$$\begin{bmatrix} i_A \\ i_B \\ i_C \end{bmatrix} = C \begin{bmatrix} 2 & 0 \\ 1 & \sqrt{3} \\ -1 & \sqrt{3} \end{bmatrix} \begin{bmatrix} \cos\gamma_1 z_0 \\ \sin\gamma_1 z_0 \end{bmatrix} f_{zd}. \qquad (2)$$

The variables i_A, i_B, and i_C correspond to the three-phase currents applied to the coils. The parameter γ_1 is the magnitude of the spatial wave number of the first harmonic, $\gamma_1 = |2\pi/l|$, where l is the pitch of the motor (63.3 mm). The relative lateral displacement of the mover with respect to the stator is denoted z_0, and f_{zd} is the desired axial thrust.

Equation (2) provides three equations for only one unknown, C, as the currents are given, and the displacement and force can be readily determined. To find an appropriate value for C, analytical and experimental procedures were executed. In each instance, balanced three-phase currents and a displacement (z_0) were fixed. Upon statistical investigation of the data for C, the median value was selected. Once C is determined, the controller output can be converted to the three desired output currents as follows. The output from the controller is force, which is multiplied by the geometric quotient C and the appropriate sinusoidal displacement dependency as in (2). The maximum swing of the current to the coils is ±3 A, proportional to the output voltage from the controller board. Hence the transconductance

Table 1. Analytical force output.

	Coil in Phase A		Coil in Phase B		Coil in Phase C	
Magnet	Distance	Force/ Current	Distance	Force/ Current	Distance	Force/ Current
	(mm)	(N/A)	(mm)	(N/A)	(mm)	(N/A)
1	-36.55	0.00	-26.00	-0.05	-15.45	-0.23
2	-27.03	-0.05	-16.48	-0.20	-5.93	-0.58
3	-4.90	-0.53	5.65	-0.57	16.20	-0.20
4	4.63	-0.52	15.18	-0.24	25.73	-0.06
5	26.75	-0.05	37.30	0.00	47.85	0.00
6	48.85	0.00	59.40	0.00	69.95	0.00
Force/Current (N/A)		-1.16		-1.06		-1.07
Multiplied by 3 Coils		-3.47		-3.17		-3.21
Current to Coils (A)		-3.00		-3.00		-3.00
Force per Phase (N)		10.40		9.51		9.62
Total Force (N)			29.60			

amplifier gain is 0.333 A/V.

To analytically determine the force capabilities of the motor, the individual contributions for each magnet-coil interaction must be summed. Since the pitch of the coils matches the pitch of the magnets, the force contribution from each coil in a single phase is identical. Thus the force per current for each phase is multiplied by three, as there are three coils in each phase. From Fig. 4, it is clear that for magnets beyond 30 mm, the force contribution is negligible, so only the six closest magnets to each coil are taken into consideration.

Table 1 enumerates the force contributions between the six nearest magnets and a single coil in each phase. The magnet number corresponds to the magnets as labeled in Fig. 2. The force per current is summed for each representative coil, then multiplied by three because there are three coils in each phase. This force-per-current value for each phase is multiplied by the current sent through that phase to find the force output. The total force is found by adding the force outputs from each phase. Table 1 represents the position and current condition for maximum force output, which relaxes the balanced three-phase condition. The maximum force is determined to be 29.6 N. With the balanced three-phase condition in place, the maximum force is 19.4 N.

2.5. Experimental setup and instrumentation

The experimental setup is depicted in Fig. 5. The linear variable differential transformer (LVDT) is connected to the mover of the motor through a threaded rod. The LVDT outputs the analog position signal to the conditioning circuit, which shifts and filters it, then sends it to an analog-to-digital (A/D) channel of the DS1104 controller board. The controller board processes the position signal, and outputs appropriate control signals to the PWM amplifiers. The amplifiers then generate currents proportional to the voltage, which power the coils and exert force to the permanent magnets fixed in the mover, causing translation. The following subsections

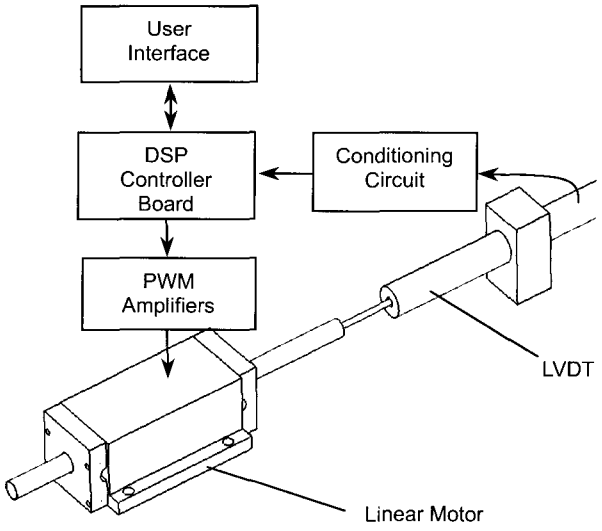

Fig. 5. Experimental setup. The position signal read by the LVDT passes through the conditioning circuit to the controller board, which compares it with the desired value and ouputs signals to the amplifiers which power the coils, inducing translation.

detail the critical instrumentation used in the setup.

1) LVDT

The LVDT is comprised of a single primary coil of wire with secondary coils placed on either side of the primary coil. The zero position is set by adding a constant to the input in Simulink. The LVDT is Schaevitz part #02560995-000, model 4000 DC-SE. The analog output swing is 0–5 VDC, with a travel range of 10 cm. The noise is listed as less than 10 mV rms.

2) Conditioning Circuit

A signal conditioning circuit comprised of two operational amplifiers, a voltage regulator, and several resistors was constructed to shift the output voltage of the LVDT to match the input swing of the A/D channel with which it was interfaced. This circuit was necessary to maximize the position resolution. An anti-aliasing filter in the form of a first-order RC filter with a cut-off frequency of 400 Hz was also implemented.

3) DS1104 Controller Board

The DS1104 digital-signal-processing (DSP) controller board from dSPACE provides the interface between the controller and the motor. The DSP board has a 250-MHz Power PC 603e with Texas Instruments' DSP TMS320F240 chip. It contains four 16-bit A/D channels, four 12-bit A/D channels, eight 16-bit digital-to-analog (D/A) channels, and other digital input/output interfaces. We developed a user-friendly interface to provide system control and observation with the provided Control Desk

Developer along with Matlab/Simulink. One of the 16-bit A/D channels was used to transmit data from the sensor to the computer, sampling at 5 kHz. Three D/A channels were used to output data to the three pulse-width- modulation (PWM) amplifiers.

4) PWM Amplifiers

Three PWM amplifiers (Model 12A8K from Advanced Motion Controls) power the three phase currents. Each amplifier is capable of outputting 6 A continuously, which is twice as large as the maximum current rating of our tubular motor.

3. CONTROLLER DESIGN AND IMPLEMENTATION

In this section, the system modeling and controller development is discussed. Various controllers were developed to better achieve the desired performance characteristics for robotics applications. In each case, a classical lead-lag controller is the backbone of the solution. Gain scheduling is implemented to decrease the effect of the dead-band region of the response. Two primary performance requirement sets are entertained. The first requirement set is for a fast rise time with minimal position noise, which is what is required for many precision positioning applications. The second requirement set is for little or no overshoot, as may be required in some robotics applications when significant overshoot may imply undesirable impact.

3.1. Plant model

The LVDT allows its iron core to slide without contact, thus contributing no friction forces on the system. The nylon bearings located at both ends of the linear motor contribute very little friction to the system, and friction is therefore neglected initially from the system model. Thus the system can be modeled as a pure mass. The mass of the mover measured 175 g on a precision scale. The corresponding plant transfer function is

$$\frac{Y(s)}{f(s)} = \frac{1}{0.175s^2}. \tag{3}$$

3.2. Controller design

Since the system is modeled as a pure mass, the model is marginally stable. To decrease the rise time and add damping, a lead compensator was added. To improve the steady-state performance of the system, a lag compensator was included as well. To have acceptable damping, the system should have a phase margin greater than 60°. For zero steady-state error, a pole is placed at the origin of the s-plane. The required minimum rise time limits the lower bound of the system gain, however in practice the actual gain was much higher than this bound. Thus, the system gain, remaining pole and zeros were determined through many trial-and-error iterations. The Matlab function 'rltool' was used to finalize the controller parameters to achieve appropriate dynamic performances. Equation (4) gives the discrete-time version of a controller with a 5-kHz sampling frequency.

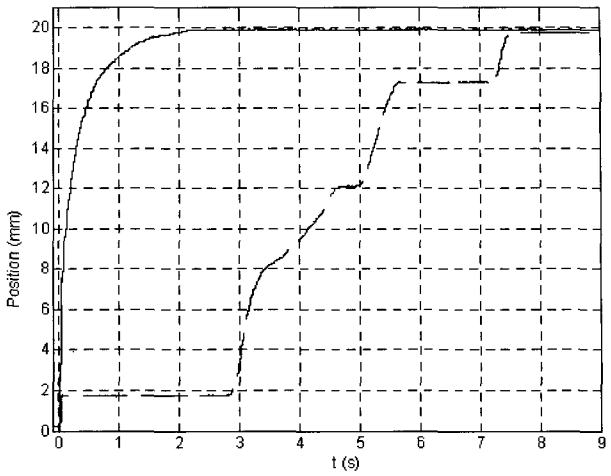

Fig. 6. System response to 20-mm step before gain scheduling (dashed line) and after gain scheduling (solid line).

$$1.7\times10^5 \frac{(z-0.996)(z-0.9608)}{(z-1)(z-0.67032)}. \tag{4}$$

This controller yields a phase margin of 73.6° at the crossover frequency of 40 Hz, which is applicable for applications requiring a fast step response with 20–30% overshoot acceptable. Many other controllers were also developed and their performance was inspected to determine their applicability to particular robotics applications, such as no-overshoot applications or high-speed point-to-point positioning.

3.3. Gain scheduling

In experimental step responses, to be discussed in Section 4, the two most significant problems were high amplitude noise in the system, and a significant dead-band region present. The noise was significantly reduced with software filtering, component redesign, and fixing the motor on a vibration isolation table. The dead-band region present in system responses is due to nonlinear friction present in the system. When the motor moves to a point near the desired position, it takes substantial time for it to make another move towards the final position. A pole in the controller placed at the origin of the s-plane sums the error. Because the motor is near the final position, the error is small, however, it takes time for the controller

to accumulate commanding currents large enough for the motor to overcome the friction, resulting in a significant time delay.

In order to eliminate this dead-band region, gain scheduling was implemented. A lookup table was included in the Simulink controller that effectively increased the gain by a factor when the position was within a small threshold on either side of the desired position. A 'dead' area within 50 μm was allowed to remain in order to prevent exacerbation of the noise when near the desired final value. Fig. 6 gives the system response to a 20-mm input command, with and without gain scheduling implemented. The controller used here is specifically designed to reach the desired position without overshoot, however this caused it to be slow, especially for large steps. Through this method of gain scheduling, the effect of the dead-band region was significantly diminished, with the rise time reduced from over 7 s to less than 0.8 s.

4. EXPERMENTAL RESULTS

In order to determine the widest scope of applications for which the motor is appropriate, numerous experiments were performed to test its capabilities. Several controller modifications were introduced to optimize control for the different applications. These modifications include filtering, gain scheduling, and path planning. Note that all data for the position reading is taken after filtering of the signal from the LVDT.

4.1. Experimentally determined actuation force

To experimentally find the maximum pull-out force of the motor, fixed currents were applied to the three phases of the coils and an external force was applied to the mover via a hanging load and pulley, as shown in Fig. 7. The load was increased incrementally by adding small weights to the hanging mass until the force reached the motor's pull-out force, and the motor released the load to fall. The last added weight was removed, and the remaining mass was resolved on a scale. This mass was multiplied by the gravitational constant to determine the force. When the maximum current (3 A) was applied to each phase of coils, the pullout force was found to be 26.3 N. This value correlates with the theoretically-predicted value of 29.6 N, found using (1).

4.2. Step responses

The step response of a linear actuator is a useful tool to gauge its performance in point-to-point maneuverability. Many applications require an actuator to move from one position to another, in as fast a time as possible. Other important characteristics are the percent overshoot, settling time, and steady-state error.

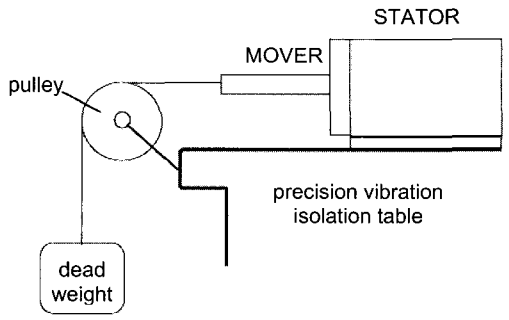

Fig. 7. Experimental setup to determine maximum pullout force. The load hangs from a string that is held by the motor via a pulley. Load is incrementally increased to the hanging mass by adding small weights.

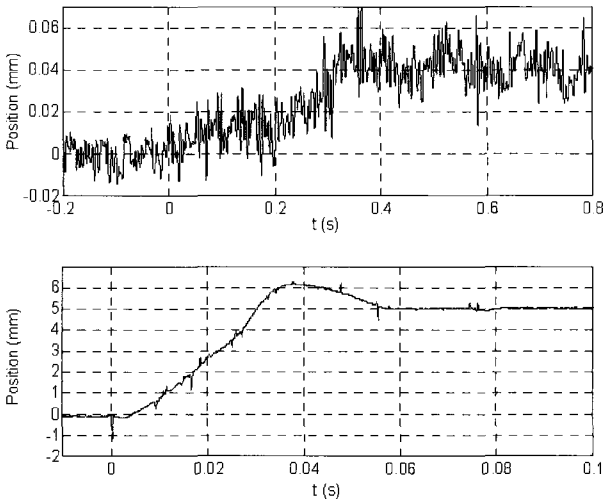

Fig. 8. System response to 40-μm step (top) and to a 5-mm step (bottom).

The first plot in Fig. 8 shows the system step response to a 40-μm step command. The rise time is less than 0.3 s, and the settling time is about 0.4 s. These transient responses are rather slow considering the 40-Hz crossover frequency of the control system. It is believed to be that the friction in the nylon bearings and the dead-band slowed this microscale motion. The second plot in Fig. 8 shows a 5-mm step response. The rise time is about 20 ms and the settling time is about 60 ms without significant nonlinear effects.

It is clear that the positioning resolution of the system is better than 20 μm. The limitation on the position resolution arises from the noise prevalent in the LVDT sensor and its electronics. Incorporation of a sensor capable of finer precision would yield significantly better position resolution from the motor.

Fig. 9 illustrates the system response to much larger steps, ranging from 2 to 5 cm with 1-cm increment.

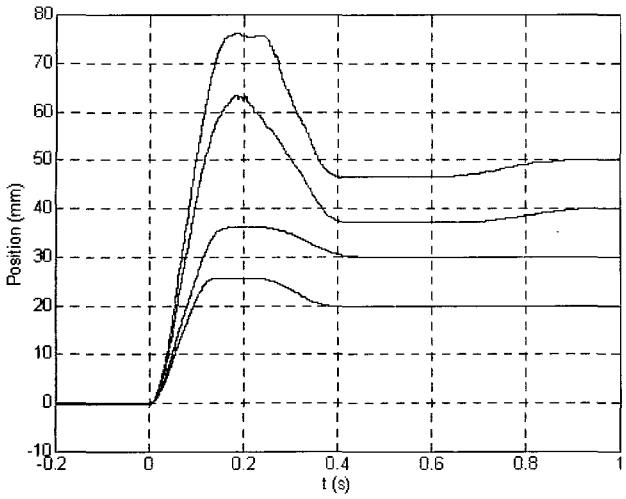

Fig. 9. System response to input steps ranging from 2 to 5 cm, in 1 cm increments.

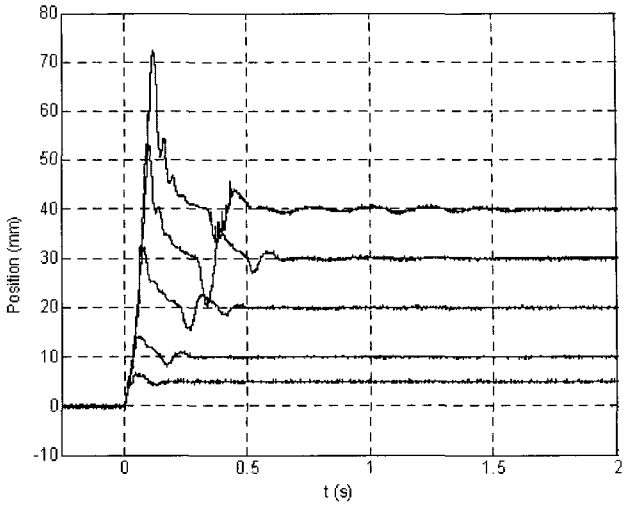

Fig. 10. Loaded system step responses with step sizes of 5 mm, and 1–4 cm, with 1-cm increment, with 5-N external load applied.

In these steps the rise time is less than 0.1 s, with settling times ranging from 0.2 to 1 s, and overshoots from 20 to 55%. The non-uniformity of the rise and settling times is considered to result from the unmodeled nonlinearity (e.g. the dead-band friction in the bearings) existing in the system.

An important attribute of the motor is its ability to perform under an added load. To that end, several step responses were taken with a load of 5 N added to the system through a pulley, as given in Fig. 7. Fig. 10 gives the loaded system response to steps ranging from 5 mm to 5 cm in the direction opposite to the applied load. The rise times range from 30 to 100 ms. The settling times range from 0.15 to 1.4 s, and the overshoot ranges from 30 to 80%. The significant dip after the initial overshoot is due to the slack that develops in the rope after the motor has raised the mass. This test validates the motor for use in applications requiring steps with an added load.

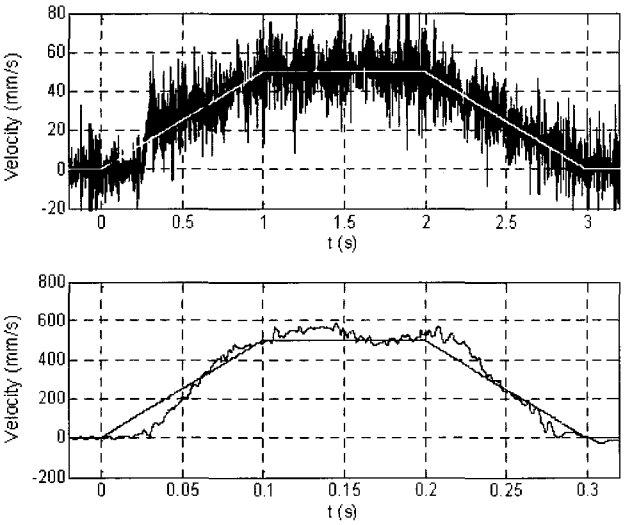

Fig. 11. Motor response to velocity profile input commands. In the upper plot, the motor reaches a top speed of 50 mm/s. In the lower plot, the top speed reached is 500 mm/s. Note the time and velocity scales.

4.3. Velocity profile tracking

Another common tool used to gauge the performance of a motor is its ability to track a certain velocity profile, e.g. a trapezoidal velocity profile. This profile consists of linearly accelerating to a desired velocity, holding that velocity for some time, then decelerating back down. The position reading from the sensor is differentiated with respect to time to determine the velocity. In each case, the mover traversed the entire 10-cm range of the system. The performance results for two experiments are given in Fig. 11, where in each case the command signal is distinguishable as the signal comprised of a few straight lines. In the first case, the maximum desired speed is 50 mm/s. The noise prevalent in the response is due to the method used to determine the velocity. Since there is already noise present in the position data from the LVDT, differentiating this data with respect to time amplifies the presence of the noise. After an initial delay, the system is capable of tracking this profile very well.

In the second plot of Fig. 11, the maximum desired speed is 500 mm/s. The motor reaches this velocity after 100 ms, corresponding to an acceleration of ½ g. The initial behavior is similar to the prior trial, with an initial delay in following the input velocity command. The damaging effects of the dead-band friction are more significant as there is less time for the system to respond. The motor still tracks this signal but does not follow as the input command as closely compared with the slower motion shown in the first plot of Fig. 11.

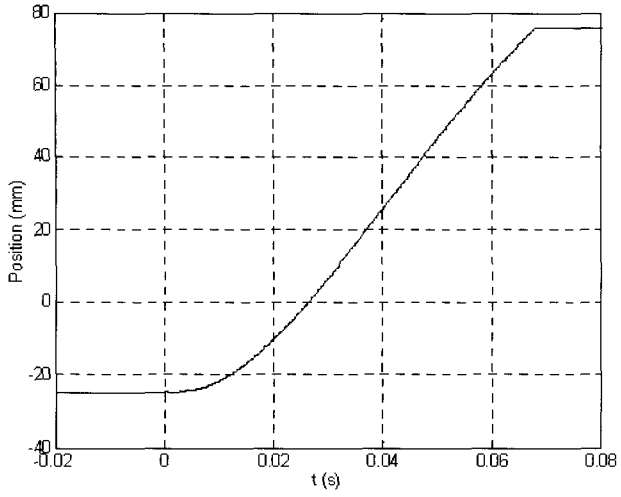

Fig. 12. High-speed traversal of entire travel range.

4.4. Traversal of full travel range

Experiments were performed to demonstrate the capabilities of the motor traversing its entire 10-cm travel range. The traversal is made in about 67 ms as given in Fig. 12, which corresponds to an average speed of about 1.5 m/s. The motor accelerates to a velocity of 1.1 m/s after the first 11 ms, corresponding to an acceleration of 100 m/s^2, or about 10 *g*. To achieve no-overshoot, as required for some robotics applications, a path planner was also implemented in which the desired position input to the system was a decaying exponential. In this case, it took approximately 2 s to traverse the entire distance.

5. CONCLUSIONS

A design for a novel direct-drive permanent-magnet tubular motor has been presented. The purpose of the motor is to provide actuation solutions to a number of robotics needs; primarily compact, fast, smooth, precision positioning. The motor is comprised of an array of axially magnetized permanent magnets fixed within a brass tube, placed within an array of cylindrical current-carrying coils. The design allows for indiscriminate length of the magnet array, allowing unlimited possible translation. A force is exerted on the permanent magnets from the coils according to the Lorentz force equation, producing translation. Commutation equations relating the three-phase currents as a function of position and output force were determined. The linear motor is operated in conjunction with a position sensor, three power amplifiers, and a controller to form a complete solution for precision actuation and control.

Lead-lag controllers were designed and implemented to increase positioning speed and reduce steady-state error and overshoot. Gain scheduling was implemented to reduce the effect of dead-band. The motor is capable of traversing the 10-cm travel range in 67 ms, which corresponds to a speed of approximately 1.5 m/s. It is capable of acceleration up to 10 *g*. The system responds to a 5-mm step command with a rise time, settling time, and overshoot of 30 ms, 20 ms, and 25%, respectively. The motor can make a 4-cm step with an added 5-N load with a rise time of 80 ms, a settling time of 1.5 s, and 80% overshoot. The motor is capable of force up to 26 N, with a 20-μm position resolution. The compact size of the motor and its capability to extend the moving part well beyond its support base suggest that it could be useful in many motion-control applications with spatially constrained environments.

REFERENCES

[1] C. S. Lovchik and M. A. Diftler, "The Robonaut hand: a dexterous robot hand for space," *Proc. of IEEE International Conference on Robotics and Automation*, vol. 2, pp. 907-912, May 1999.

[2] P.-K. Budig, "The application of linear motors," *Proc. of IEEE Power Electronics and Motion Control Conference*, vol. 3, pp. 1336-1341, August 2000.

[3] B. Lequesne, "Permanent magnet linear motors for short strokes," *IEEE Trans. on Industry Applications*, vol. 32, no. 1, pp. 161-168, January/February 1996.

[4] W.-J. Kim, D. L. Trumper, and J. H. Lang, "Modeling and vector control of planar magnetic levitator," *IEEE Trans. on Industry Applications*, vol. 34, no. 6, pp. 1254-1262, November/ December 1998.

[5] D. L. Trumper, W.- J. Kim, and M. E. Williams, "Design and analysis framework for permanent-magnet machines," *IEEE Trans. on Industry Applications*, vol. 32, no. 2, pp. 371-379, March/April 1996.

[6] K. Halbach, "Design of permanent multipole magnets with oriented rate earth cobalt material," *Nucl. Instrum. Methods*, vol. 169, no. 1, pp. 1-10, 1980.

[7] M. T. Berhan, *Implementation of a Halbach Array in a Tubular Linear Motor*, Masters' Thesis, Dept. of Mechanical Engineering, Massachusetts Institute of Technology, June 1996.

[8] W.-J. Kim, M. T. Berhan, D. L. Trumper, and J. H. Lang, "Analysis and implementation of a tubular motor with Halbach magnet array," *Proc. of the IEEE Industry Applications Society 31st Annual Meeting*, pp. 471-478, October 1996.

[9] M. Ishiyama, I. Makoto, T. Kitaoka, Y. Matsumoto, and M. Yagoto, "Linear motor," U.S. Patent and Trademark Office, Patent # 5 955 798, September 1999.

[10] Z. Q. Zhu, P. J. Hor, D. Howe, and J. Rees-Jones, "Novel linear tubular brushless permanent

magnet motor," *Proc. of IEE Eighth International Conference on Electrical Machines and Drives*, pp. 91-95, September 1997.

[11] C. M. Liaw, R. Y. Shue, H. C. Chen, and S. C. Chen, "Development of a linear brushless DC motor drive with robust position control," *IEE Proc. of Electric Power Applications*, vol. 148, no. 2, pp. 111-118, March 2001.

[12] N. C. Shieh and P. C. Tung, "Robust output tracking control of a linear DC brushless motor for transportation in manufacturing system," *IEE Proc. of Electric Power Applications*, vol. 148, no. 2, pp. 119-124, March 2001.

[13] S. Brückl, "Feed-drive system with a permanent magnet linear motor for ultra precision machine tools," *Proc. of IEEE International Conference on Power Electronics and Drive Systems*, pp. 821-826, July 1999.

[14] A. Basak and G. H. Shirkoohi, "Computation of magnetic field in DC brushless linear motors with NdFeB magnets," *IEEE Trans. on Magnetics*, vol. 26, no. 2, pp. 948-951, March 1990.

[15] G.-H. Lee, "Cylindrical linear motor having individually toothed laminated primary cores," U.S. Patent and Trademark Office, Patent # 5 844 332, December 1998.

[16] D. L. Trumper, W.-J. Kim, and M.E. Williams, "Magnetic arrays," U.S. Patent and Trademark Office, Patent # 5 631 618, May 1997.

[17] M. Ishiyama, "Linear motor equipped with a stator which is easily assembled," U.S. Patent and Trademark Office, Patent # 6 040 642, March 2000.

[18] R. Akmese and J. F. Eastham, "Dynamic performance of a brushless DC tubular drive system," *IEEE Trans. on Magnetics*, vol. 25, no 5, pp. 3269-3271, March 1989.

[19] J. F. Eastham, R. Akmese, and H. C. Lai, "Optimum design of brushless tubular linear machines," *IEEE Trans. on Magnetics*, vol. 26, no. 5, pp. 2547-2549, April 1990.

[20] B. Murphy, *Design and Construction of a Precision Linear Motor and Controller*, Masters' Thesis, Dept. of Mechanical Engineering, Texas A&M University, May 2003.

[21] H. A. Haus and J. R. Melcher, *Electromagnetic Fields and Energy*, Pretence-Hall, Inc., 1989.

[22] H. Maheshwari, *Design and Fabrication of a Maglev Linear Actuator Capable of Nanopositioning*, Masters' Thesis, Dept. of Mechanical Engineering, Texas A&M University, December 2002.

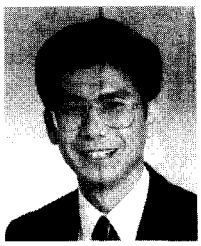

Won-jong Kim received the B.S. (*summa cum laude*) and M.S. degrees in control and instrumentation engineering from Seoul National University, Seoul, Korea, in 1989 and 1991, respectively, and the Ph.D. degree in electrical engineering and computer science from Massachusetts Institute of Technology, Cambridge, in 1997. In September 2000, he joined the Department of Mechanical Engineering, Texas A&M University, College Station, where he is currently an Assistant Professor. Following receipt of the Ph.D. degree, he was with SatCon Technology Corporation, Cambridge, MA, for three years. His teaching and research interests focus on analysis, design, and real-time control of mechatronic systems, and nanoscale engineering and technology. He holds two US patents on precision positioning systems.

Dr. Kim received the Grand Prize from the Korean Institute of Electrical Engineers' Student Paper Contest in 1988 and the Gold Prize for his doctoral work from Samsung Electronics' Humantech Thesis Prize in 1997. He was a semifinalist of the NIST's Advanced Technology Program 2000 Competition. The NASA granted him the Space Act Award in July 2002. He was appointed a Select Young Faculty Fellow by the Texas Engineering Experiment Station in September 2003. He is the Chair of the ASME Nanoscale Control Technical Panel and a member of the IEEE Nanotechnology Council. He is a senior member of IEEE and a member of ASME, ASPE, KSEA, Pi Tau Sigma, and Sigma Xi.

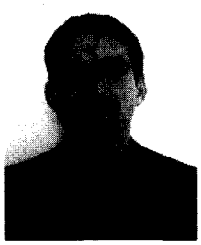

Bryan C. Murphy received the B.S. and M.S. degrees in Mechanical Engineering with an emphasis in control systems from Texas A&M University in 2001 and 2003 respectively. While at Texas A&M, he received the Summer Undergraduate Research Grant and the department's Teaching Assistant of the Year Award, 2002. In 2003, he was awarded an NSF East Asia and Pacific Program (EAP) grant, for which he spent two months researching robotics at the Pohang University of Math and Science in Pohang, Korea. In February 2004, he began work for The Boeing Company, Houston, supporting the International Space Station. Mr. Murphy's research interests include motion control systems, microcontrollers, robotics, and mechatronic systems.